# A nonlinear, geometric Hall effect without magnetic field

Nicholas B. Schade[a,b,c,1], David I. Schuster[a,b], and Sidney R. Nagel[a,b,c]

[a]Department of Physics, The University of Chicago, Chicago, IL 60637; [b]The James Franck Institute, The University of Chicago, Chicago, IL 60637; and [c]The Enrico Fermi Institute, The University of Chicago, Chicago, IL 60637

Edited by Steven M. Girvin, Yale University, New Haven, CT, and approved October 24, 2019 (received for review September 20, 2019)

**The classical Hall effect, the traditional means of determining charge-carrier sign and density in a conductor, requires a magnetic field to produce transverse voltages across a current-carrying wire. We demonstrate a use of geometry to create transverse potentials along curved paths without any magnetic field. These potentials also reflect the charge-carrier sign and density. We demonstrate this effect experimentally in curved wires where the transverse potentials are consistent with the doping and change polarity as we switch the carrier sign. In straight wires, we measure transverse potential fluctuations with random polarity demonstrating that the current follows a complex, tortuous path. This geometrically induced potential offers a sensitive characterization of inhomogeneous current flow in thin films.**

transverse potential | Hall effect | surface charge | graphene

In 1879, Edwin Hall discovered that a transverse potential appears across a current-carrying wire placed in a magnetic field (1). Physics instructors traditionally teach the Hall effect when the magnetic field is first presented in introductory electricity and magnetism as the way to distinguish the sign of the charge carriers in a conductor (2). Indeed, the Hall effect is an efficient way to disentangle the role of electron and hole conduction in semiconductors (3) and is commonly used to measure the magnitude of magnetic fields (4). Here we present a different mechanism using geometry alone, without a magnetic field, to produce a transverse voltage that also reflects the sign and density of the charge carriers. A current traveling through a curved wire must undergo centripetal acceleration to follow the curve. This acceleration occurs due to electric fields from charges distributed along the wire edges; the direction of the field must change with the sign of the carriers. No magnetic field is necessary. This observation changes the way we think about the creation of transverse potentials in wires because it is simply a geometric effect that has until now gone unnoticed.

The transverse voltage that we predict and measure is quadratic in the current. It is therefore distinct from many linear Hall effects such as the spin (5), valley (6), and anomalous (7) Hall effects. However, the geometric effect we describe should be contrasted with predictions (8) and recent measurements of a nonlinear Hall effect in nonmagnetic bilayer materials such as $WTe_2$ (9).

By 1850, Kirchhoff realized that surface charge distributions are necessary simply to confine a current inside a wire (10). Subsequently, the role of surface charges has been investigated theoretically (11–13) and experimentally using single-electron transistors (14, 15). The effect we describe is also related to how currents are confined within wires. Our experiments show that the effect can be used for sensitively probing nonhomogeneous current flow in thin films as well as systems where magnetic fields do not occur such as the bulk of a superconductor. While the effect is small, it is measurable even in bulk conductors. Using graphene wires to optimize the signal, we measure transverse potentials $\approx$0.5 mV.

In the conventional Hall effect, when an electric current $i$ of charge carriers $q$ passes through an applied magnetic field $\mathbf{B}$, the carriers experience a magnetic Lorentz force $\mathbf{F_B} = q\mathbf{v} \times \mathbf{B}$. Charge accumulates at the wire edges, as illustrated in Fig. 1*A*, until the electric field caused by these charges cancels $\mathbf{F_B}$ to create a transverse potential difference:

$$\Delta V_{\mathrm{Hall}} = \frac{iB}{tnq}. \quad [1]$$

Here $n$ is the charge-carrier density and $t$ the wire thickness along the direction of $\mathbf{B}$. A measurement of $\Delta V_{\mathrm{Hall}}$ determines $n$ and the sign of the charge carriers.

To show that magnetism is not necessary for producing transverse voltages sensitive to $n$ and the sign of $q$, we take advantage of surface charge distributions that are a result of geometry—curvature in the path of the current—rather than magnetic forces. The surface charges create a transverse component of the electric field and exert a force on the current such that it follows the wire. For a wire in the shape of a circular arc, the transverse electric force must point radially toward the circle center to accelerate the carriers centripetally; this mandates that the direction of the radial electric field (and thus the potential difference between the wire edges) depends on the sign of the current carriers, as illustrated in Fig. 1*B*. The polarity of this potential, analogous to the polarity of a Hall potential, reveals the sign of the carriers.

## Theory

Calculating this potential is straightforward. We assume the wire is a semicircular annulus with inner radius $r_{\mathrm{in}}$ and outer radius $r_{\mathrm{out}}$; the wire has a rectangular cross-section of width

### Significance

We show that electric current flowing through a curved wire produces a transverse electric potential across the wire. The potential arises because a transverse electric field must accelerate the current radially to follow the curve. This is a geometric effect in which no magnetic field is present. This potential reflects the sign and density of the current-carrying charges, properties that are traditionally obtained by applying a magnetic field to measure the Hall voltage. We experimentally observe potentials in curved graphene wires that are as large as millivolts. Even straight wires exhibit transverse voltages of geometric origin due to tortuous current paths within the wires. Thus, this nonlinear transverse-potential measurement is a probe of current paths in conductors.

Author contributions: N.B.S., D.I.S., and S.R.N. designed research; N.B.S. performed research; N.B.S. analyzed data; and N.B.S. and S.R.N. wrote the paper.

The authors declare no competing interest.

This article is a PNAS Direct Submission.



[1]To whom correspondence may be addressed. Email: nschade@uchicago.edu.

This article contains supporting information online at https://www.pnas.org/lookup/suppl/doi:10.1073/pnas.1916406116/-/DCSupplemental.

First published November 18, 2019.

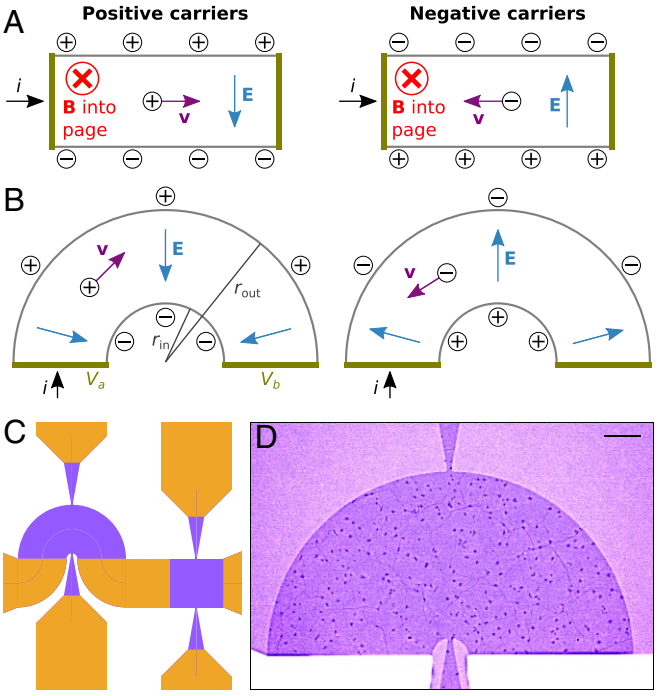


**Fig. 1.** Surface charge distributions that produce transverse potentials. (*A*) In the classical Hall effect, the directions of current, *i*, and of the magnetic field, **B**, determine the direction of the magnetic force. The surface charges produce a transverse electric field **E**. (*B*) In a curved wire without an applied magnetic field, the centripetal acceleration of the carriers is due to an electric force. Surface charges produce an electric field whose direction reveals the sign of the carriers. (*C*) Circuit for measurement of transverse potentials due to wire geometry. Orange regions are metal and purple regions are exposed graphene. (*D*) Optical micrograph of the curved graphene wire in a completed device. Graphene electrodes are visible in center at top and bottom. (Scale bar, 20 μm.)

$w \equiv (r_{\rm out} - r_{\rm in})$ and thickness $t$. We force the radial edges of the half annulus to be equipotentials, as illustrated in Fig. 1*B*, with potential difference $\mathcal{E} = V_a - V_b$. Symmetry requires that the current density vector field is purely azimuthal, such that the charge carriers on average follow semicircular trajectories. We assume that the conductivity $\sigma$ and carrier density $n$ are uniform and that all charge carriers have the same mass $m$ and charge $q$.

Unless the wire is a superconductor, the current-density magnitude, $j(r)$, is equal to the longitudinal (azimuthal) component of the electric field, $E_\theta = \mathcal{E}/(\pi r)$, times the conductivity: $j(r) = \sigma\mathcal{E}/(\pi r)$. The transverse (i.e., radial) component, $E_r$, provides the force necessary for the carriers to follow circular paths on average.

In the curved wire that we consider, the magnitude of the local drift velocity $\langle v\rangle$ of the carriers is proportional to the current density, $\langle v\rangle = j/nq$, and the force for keeping these particles in a circular orbit of radius $r$ is $F = m\langle v\rangle^2/r = E_r q$. The radial electric field is thus

$$E_r(r) = -\frac{dV(r)}{dr} = \frac{m\,[j(r)]^2}{n^2 q^3 r}, \qquad [2]$$

where $V(r)$ is the transverse electrostatic potential. This can be integrated across the width of the wire, $w$, to find $\Delta V_{\rm geom} \equiv V_{\rm out} - V_{\rm in}$,

$$\Delta V_{\rm geom} = \left[\frac{r_{\rm in}^{-2} - r_{\rm out}^{-2}}{2t^2\,(\ln(r_{\rm out}/r_{\rm in}))^2}\right]\left(\frac{m}{n^2 q^3}\right) i^2 \qquad [3]$$

$$\approx \left[\frac{1}{r_{\rm in} w t^2}\right]\left(\frac{m}{n^2 q^3}\right) i^2 \ \text{ in limit } w \ll r_{\rm in} \qquad [4]$$

$$\approx \left[\frac{w}{r_{\rm in}}\right]\left(\frac{m}{n^2 q^3}\right)\langle j\rangle^2 \ \text{ in limit } w \ll r_{\rm in}. \qquad [5]$$

The terms in square brackets depend only on the wire geometry. The expression in Eq. **3** is exact for a wire of any width; the approximations in Eqs. **4** and **5** are valid in the narrow-wire limit, $w \ll r_{\rm in}$, with $\langle j\rangle = i/wt$ being the average current density. As in the Hall effect, the potential $\Delta V_{\rm geom}$ is an odd power of the charge $q$, which means that the sign of $q$ can be determined.

We note that this result, essentially due to momentum conservation, is equally valid in the diffusive limit where the charge carriers experience collisions that randomize their velocities. Momentum conservation still dictates that the electric field must include a radial component as in the Drude model (16),

$$\frac{d}{dt}\langle \mathbf{p}(t)\rangle = q\mathbf{E} - \frac{\langle \mathbf{p}(t)\rangle}{\tau}. \qquad [6]$$

In steady state, with a constant azimuthal current, the left side of Eq. **6** must equal the transverse force necessary to keep the current traveling along a circular arc. This leads to Eq. **2**. See *SI Appendix* for details.

There are 2 significant differences between this transverse potential and the Hall effect, however. The first one is that the mass of the carriers, $m$, enters into the expression for the potential difference. The second difference is that $\Delta V_{\rm geom}$ is quadratic, rather than linear, in the current, $i$.

## Experimental Validation

**Circuit Design.** To maximize the signal $\Delta V_{\rm geom}$, we need high current $i$ (or current density $j$) and low carrier density $n$. It is advantageous to use a conductor whose charge-carrier sign and density can be modulated to check whether the signal and carriers change sign concurrently. Monolayer graphene satisfies these conditions (17).

Due to graphene's electronic band structure, as the Fermi energy approaches the Dirac point, the effective mass $m^*$ of the charge carriers vanishes and the carriers behave like relativistic Dirac particles (18). The effective mass is given by $m^* = (\hbar/v_F)\sqrt{\pi n_{\rm 2D}}$, where $v_F$ is the Fermi velocity, $\hbar$ is the reduced Planck constant, and $n_{\rm 2D} = nt$ is the 2D carrier density (19, 20). By applying a gate voltage to place the Fermi energy far from the Dirac point, we ensure that the charge carriers in our circuits have a nonzero effective mass. Additionally, we design our wires to be orders of magnitude longer and wider than the electronic mean free path in room-temperature graphene (21), which means that the nonrelativistic, diffusive transport model should be applicable to our experiments.

Our circuit, illustrated in Fig. 1*C*, consists of a curved graphene wire with measurement leads on either side and a straight graphene wire as a control. We use graphene grown by chemical vapor deposition and transferred by the manufacturer (Graphenea, grain size ≤20 μm) to a doped silicon wafer with a 300-nm oxide gap. We use photolithography, electron-beam evaporation, and plasma etching to pattern the graphene and to place Ti/Au contacts on it, as shown in Fig. 1*D*. (See *Materials and Methods* for a detailed nanofabrication procedure.) We control the sign and density of the carriers in the graphene by applying a back-gate voltage $V_{\rm bg}$ to the silicon. As initially fabricated, the samples are highly doped; we current-anneal (22) them to cross the Dirac point at $V_{\rm bg} < 100$ V.

The fact that the signal is quadratic in the current may be exploited to remove several potential sources of measurement error. The $i^2$ dependence means that an ac current at frequency

$\omega$ produces a transverse potential at frequency $2\omega$. We use a lock-in amplifier to measure the potential at $2\omega$ while filtering out potentials at $\omega$. A Hall potential due to a dc magnetic field, such as that of the Earth, will appear at $\omega$ and thus can be safely ignored. The potential drop due to the longitudinal electric field component within the wire, $E_\theta$, likewise occurs at $\omega$, so we need not worry about imperfect alignment of transverse measurement leads. By checking that $\Delta V_{\rm geom}$ is proportional to $i^2$, we ensure that any $2\omega$ harmonics in the current do not contribute to the signal. Fluctuations in the conductor's resistivity due to Joule heating give rise to longitudinal oscillations in the potential that occur at $3\omega$ and higher harmonics, but not at $2\omega$. (See *SI Appendix* for details.)

Two extraneous sources of a $2\omega$ signal are due to 1) the Hall voltage from a current-induced magnetic field and 2) the Seebeck effect. In *SI Appendix* we describe how we have minimized their contribution so that they do not affect our results.

## Results

We measured the potential difference, $\Delta V_{\rm geom}$, across the curved wires in our samples. In all of the samples, without any current annealing and at $V_{\rm bg}=0$, $\Delta V_{\rm geom}$ is positive, corresponding to positive charge carriers. This is what is expected in graphene on a $SiO_2$ substrate (15, 17, 23). We fitted the measured transverse potentials to a power $\beta$ of the current amplitude, $|\Delta V_{\rm geom}| \propto i^\beta$, and we find $\langle\beta\rangle = 2.00 \pm 0.11$. This confirms that the measured potential rises quadratically with the current, as shown in Fig. 2*A*. There is significant scatter in the signal magnitude between samples as shown in Fig. 2*B*. For a driving voltage $\mathcal{E} = 1.00$ V, the current is $i \approx 370 \pm 130$ μA and the average magnitude of the signal is $\langle \Delta V_{\rm geom}\rangle \approx 0.46$ mV. Using Eq. **3** and averaging over the samples, we measure $\langle m/(n^2 t^2 q^3)\rangle \approx 5\times 10^{-6}$ kg m$^4$·C$^{-3}$.

After current annealing, we can apply a back-gate voltage $V_{\rm bg}$ to the sample and move the Fermi level to the other side of the Dirac point where the charge of the carriers has the opposite sign. We find that $\Delta V_{\rm geom}$ changes sign at a back-gate voltage close to that of the conductance minimum, as shown in Fig. 2*C*. This confirms that this measurement determines the sign of the charge carriers using only geometry. [This behavior shows hysteresis with the direction of the $V_{\rm bg}$ sweep, as is typical of electrical properties of graphene (23).] Rather than showing a singularity, $\Delta V_{\rm geom}$ passes smoothly through zero near the Dirac point. This is consistent with prior observations that in graphene samples near the Dirac point, inhomogeneities and defects make the graphene behave as a random assortment of electron and hole puddles rather than as a uniform material with $n \approx 0$ (15, 24–26).

Because our samples are thin, the current $i$ is small even though the current density $j$ is very large. Therefore, the magnitude of the Hall-effect contribution from a current-induced magnetic field should be (*SI Appendix*, Fig. S3) at least 20 times smaller than the signal we observe and the prediction of Eq. **3**. We checked (*SI Appendix*) that $\Delta V_{\rm straight}$ is not due to the Seebeck effect by varying the length of the graphene voltage-measuring leads. We also measured the second harmonic in the driving current and found that it is too small to account for the $2\omega$ transverse potential that we observe.

The sign of the potential difference, $\Delta V_{\rm straight}$, between the 2 sides of the straight wire, is not picked out by the curvature of the wire. However, we still find a signal whose phase is either $\phi = 0$ or $\phi = \pi$, as shown in Fig. 2*B*. The average signal over many samples $\langle \Delta V_{\rm straight}\rangle \approx 0$, but in a single sample, the magnitude of the signal in the straight section can be comparable to, but usually smaller than, that in the curved section. We find $\langle|\Delta V_{\rm straight}|\rangle \approx 0.35\,\langle|\Delta V_{\rm geom}|\rangle$. As we sweep $V_{\rm bg}$ in a sample that has been current annealed, $\Delta V_{\rm straight}$ changes sign (just as does $\Delta V_{\rm geom}$), as shown in Fig. 2*D*.

We measured $\Delta V_{\rm straight}$ from a long straight wire with 8 pairs of electrodes across it, illustrated in Fig. 2*E*. We average over 4 long-wire samples and find that the magnitude of $\Delta V_{\rm straight}$ falls off with $d$, the distance from where the graphene makes contact with the metal source and drain as shown in Fig. 2*F*. The potential drops by nearly 2 orders of magnitude from near the leads, where $d \approx 10$ μm, to the center, where $d \approx 500$ μm.

## Discussion

It is unexpected that there is a significant signal across a straight section of wire. The sign of this voltage varies from place to place along the wire and in different samples and its magnitude is smaller than, but comparable to, that in the curved section. We conclude that the reason for this behavior is that the current paths are not homogeneous. The signal observed in the straight sections is thus due to the current taking a meandering path along the wire.

To rationalize the decrease of $\Delta V_{\rm straight}$ from the ends of the wire, we assume that the current is injected from the Ti/Au leads into the graphene at localized points; the current then fans out as it moves down the wire. This is consistent with studies showing that metal contacts introduce inhomogeneous doping (25) and that contact may be poor due to surface impurities on the graphene (15, 27). Photocurrent mapping of graphene transistors has revealed irregular electrostatic potential landscapes, including at the metal contacts and along the edges (24). As the current flows down the wire, it expands to fill more of the wire's width. Because the signal is quadratic in the current density, for fixed total current, the smaller the width, the larger will be the signal.

This interpretation also offers an explanation for the large measured magnitude of $\langle \Delta V_{\rm geom}\rangle$. If the mass in Eq. **3** is taken to be the bare mass of the electron with charge $q = e$, our data suggest a carrier density $n_{\rm 2D} \approx 10^{12}$ cm$^{-2}$, which is one-tenth the value expected for our doping level (17). Using the effective mass of the carriers would give an even smaller value for $n_{\rm 2D}$. However, if the current paths are not given by the wire width, $w$, but rather by the heterogeneity of the conductivity, then we can account for the observed large value of $\langle \Delta V_{\rm geom}\rangle$ by using a smaller width in Eq. **3**.

There is considerable evidence that currents in thin metal films (28, 29) and in 2D conductors such as graphene are not uniform throughout the wires. In graphene this has been ascribed to scattering at grain boundaries (30), as well as to charge puddles (15, 26) and local strains (31, 32). Graphene's electrical properties are anisotropic, depending on the lattice orientation (33), and they require a conductivity tensor (34) for a detailed analysis. Since our wires are large enough that they are polycrystalline, these features would manifest themselves as resistivity inhomogeneities. The measurement of a transverse $2\omega$ signal, $\Delta V_{\rm straight}$, is an elegant probe of the tortuous current path.

## Conclusion

We have demonstrated a transverse voltage across a current-carrying wire due to geometry alone. In the classical Hall effect, a magnetic field curves the paths of charge carriers inside a straight wire so that charges accumulate on the wire edges transverse to the current. In the geometric analog, we do not bend the paths of the carriers but instead bend the conductor itself to create a purely geometric effect. The observed signal is consistent with a prediction from elementary mechanics and electrodynamics.

We observe signals even in straight wires. Although the wires themselves are straight, the internal current paths are not. Just as for curved wires, charge distributions are necessary to confine currents to any heterogeneous path. The nonlinear transverse voltage offers an additional technique for studying such heterogeneities.

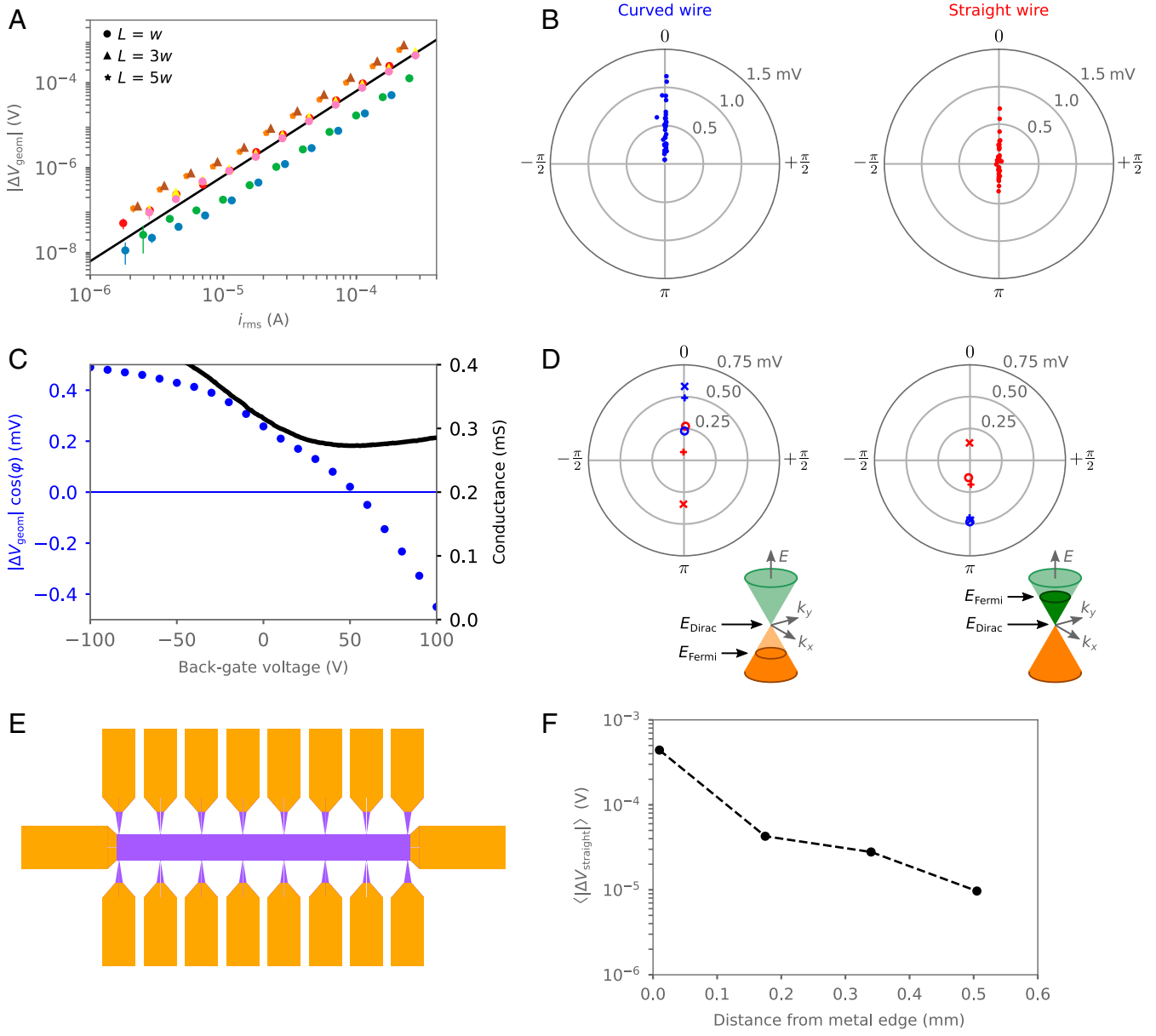


**Fig. 2.** Measured transverse potentials in graphene wires. (*A*) Signal across curved wire versus current. Colors correspond to different samples, each with $r_{in} = 10$ μm, $r_{out} = 100$ μm, and graphene measurement leads of length $L \geq 90$ μm. Black line, average of power-law fits to individual data sets, has slope = 2.0. (*B*) Signals from curved (blue) and straight (red) wires in 34 samples at an average current $\langle i_{rms} \rangle \approx 370$ μA. The radius and angle represent the magnitude and phase of the measurement. Error bars are smaller than data markers. (*C*) Signal across a curved wire (blue) and circuit's conductance (black) versus $V_{bg}$ after current annealing. (*D*) Measurements from curved wires when the Fermi level is below (*Left*) or above (*Right*) the Dirac point, controlled by changing $V_{bg}$ after current annealing. Symbols correspond to different samples. For a curved wire phase $\phi = 0$ indicates positive charge carriers. (*E*) Long-wire design with 8 pairs of measurement leads. (*F*) Signal versus distance from the metal edges at either end of the straight wire, averaged across back-gate voltage sweeps from −100 V to +100 V in 4 samples.

An important difference between the classical Hall effect and the geometric effect that we have demonstrated is that the latter depends on the mass of the charge carriers. If the relevant mass in Eq. **3** is the effective mass, then this transverse potential represents a simple way of measuring the effective mass in wires where current path tortuosity is negligible. Alternative methods of measuring the effective mass of charge carriers in graphene are nontrivial (19, 20).

Recent work (9) has found a nonlinear Hall effect due to an induced Berry curvature (35) in bilayer conductors. Such an effect is not expected to occur in a single-layer material such as graphene and is not predicted to depend on the wire curvature. Our purely geometric effect can contribute to the signals found in those experiments and in turn those effects, if present, could masquerade as a geometric effect.

Low-temperature quantum Hall effects arise due to time-reversal symmetry breaking in a magnetic field. In the presence of quantum interactions, the magnetic Hall effect becomes particularly remarkable; it would be interesting to consider whether any striking quantum effects could be observed at very low temperatures due to wire geometry alone.

## Materials and Methods

**Circuit Fabrication.** We begin with CVD graphene that has already been transferred by the manufacturer (Graphenea) to a doped silicon wafer with a 300-nm $SiO_2$ gap and diced to 10-mm × 10-mm chips in a class 1,000

cleanroom. To improve adhesion between the graphene and the oxide substrate, we anneal the samples at 300 °C in nitrogen for at least 6 h using a Gemstar ALD (Arradiance).

We use the cleanroom in the Pritzker Nanofabrication Facility at the University of Chicago for our photolithography procedure. Our first round of photolithography is for the metal portions in our circuit designs. We first spin LOR 3A (MicroChem) onto the graphene at 500 rpm for 10 s and then at 3,000 rpm for 45 s, for an undercut during development. We then bake the sample at 180 °C for 5 min. We next spin AZ 1512 photoresist (Clariant) onto the sample at 500 rpm for 10 s and then at 4,500 rpm for 45 s and bake it at 115 °C for 1 min. We use a Heidelberg MLA150 Direct Write Lithographer to expose the pattern for our metal pads onto the chip, using a 405-nm laser and a dose of 100 mJ/cm$^2$. We develop the photoresist in AZ 300 MIF (Clariant) under gentle agitation for 1 min and then transfer it to deionized water for 1 min. We immediately dry the sample with nitrogen.

We use electron-beam evaporation (Angstrom Nexdep) to deposit a layer of metal onto the substrate for the electrode pads. We first deposit 2 nm of titanium (0.5 Å/s) and then 50 nm of gold (1.0 Å/s). We perform liftoff by submerging it overnight in AZ NMP (Clariant) at room temperature. The next morning, we rinse the sample with acetone (Fisher/VWR) and isopropyl alcohol (Fisher/VWR) and then dry it with nitrogen. We are careful to prevent the chip from drying out while it is exposed to acetone.

We next perform another round of photolithography to pattern the graphene itself. We spin poly(methyl methacrylate) (495 PMMA A 4; MicroChem) onto the substrate at 500 rpm for 10 s and then at 4,000 rpm for 60 s. We bake the sample at 145 °C for 5 min. Next we spin AZ 1512 photoresist onto the sample again at 500 rpm for 10 s and then at 4,500 rpm for 45 s. We bake the sample at 115 °C for 1 min. Using the direct write lithographer once again, we align to our previous pattern and then expose an inverted pattern for the graphene and metal portions of the circuits, using the 405-nm laser and a dose of 100 mJ/cm$^2$. During this step, we expose the areas where the graphene will ultimately be removed. We develop the photoresist with the same steps that we use in our first round of photolithography.

We use oxygen plasma etching (YES CV200 Oxygen Plasma Strip/Descum System) to remove the exposed PMMA layer and to remove the graphene once it is exposed. Using 50 sccm of oxygen, we etch at 400 W for 80 s. We inspect it under an optical microscope afterward to determine whether the graphene has been completely removed from the exposed areas. If it has not, we etch for 20 s or 40 s longer. Finally, we strip off the unexposed photoresist and PMMA by submerging the sample vertically in acetone for at least 6 h. Afterward, we rinse the sample with isopropyl alcohol and dry it with nitrogen.

We inspect each device on the chip under an optical microscope to make sure that the metal and graphene regions are intact and well aligned. We vacuum seal the chips for storage under low vacuum once fabrication is complete.

**Current Annealing.** As initially fabricated, the samples are highly doped; the Fermi level is far from the Dirac point. Under these conditions it is impractical to move the Fermi level to the other side of the Dirac point by applying a back-gate voltage. However, we can current anneal (22) the samples by injecting a current of $i \approx 3$ mA ($\langle j \rangle \approx 10^7$ A/cm$^2$). To do this, we apply 10.0 V between the source and drain of the device for at least 2.5 h and typically overnight, while the sample is exposed to air. Once this is done, the back-gate voltage corresponding to the graphene conductance minimum typically falls within the range of 0 to +100 V, so we can access the other side of the Dirac point by using a back-gate voltage less than +100 V.

**Electrical Measurements.** We perform electrical measurements on the graphene circuits using a probe station where the samples are exposed to air at room temperature. We use an SR830 lock-in amplifier (Stanford Research Systems) for transverse potential measurements at frequencies between 10 Hz and 250 Hz. To measure the resistance of the graphene wires, we use a Model SR570 Low-Noise Current Preamplifier (Stanford Research Systems) and a BNC-2110 Shielded Connector Accessory (National Instruments). We control the back-gate voltage using an HP 6827A Bipolar Power Supply/Amplifier.

**Data Availability.** All data needed to evaluate the conclusions in this paper are present in the main text and in *SI Appendix*.

**ACKNOWLEDGMENTS.** We are particularly grateful to Khá-Î Tô who worked on the early stages of this project and to Lujie Huang who gave important advice about nanofabrication with graphene. We thank Jiwoong Park's group (J. Park, K.-H. Lee, J.-U. Lee, and P. Poddar) as well as G. Koolstra, N. Earnest, S. Chakram, and F. Tang for technical assistance. We thank P. B. Littlewood, C. Panagopoulos, C. R. Dean, and D. T. Son for helpful discussions. This work was supported by the National Science Foundation (NSF) Materials Research Science and Engineering Centers Program DMR-1420709 and NSF DMR-1404841. This work made use of the Pritzker Nanofabrication Facility of the Institute for Molecular Engineering at The University of Chicago, which receives support from the Soft and Hybrid Nanotechnology Experimental Resource (NSF ECCS-1542205), a node of the NSF's National Nanotechnology Coordinated Infrastructure.

1. E. H. Hall, On a new action of the magnet on electric currents. *Am. J. Math.* **2**, 287–292 (1879).
2. E. M. Purcell, *Electricity and Magnetism* (Berkeley Physics Course, McGraw-Hill, New York, NY, ed. 2, 1985), pp. 241–245.
3. G. Busch, Early history of the physics and chemistry of semiconductors-from doubts to fact in a hundred years. *Eur. J. Phys.* **10**, 254–264 (1989).
4. E. Ramsden, *Hall-Effect Sensors: Theory and Applications* (Elsevier/Newnes, Amsterdam, The Netherlands, ed. 2, 2006).
5. M. I. Dyakonov, V. I. Perel, Current-induced spin orientation of electrons in semiconductors. *Phys. Lett. A* **35**, 459–460 (1971).
6. K. F. Mak, K. L. McGill, J. Park, P. L. McEuen, The valley Hall effect in $MoS_2$ transistors. *Science* **344**, 1489–1492 (2014).
7. N. Nagaosa, J. Sinova, S. Onoda, A. H. MacDonald, N. P. Ong, Anomalous Hall effect. *Rev. Mod. Phys.* **82**, 1539–1592 (2010).
8. I. Sodemann, L. Fu, Quantum nonlinear Hall effect induced by Berry curvature dipole in time-reversal invariant materials. *Phys. Rev. Lett.* **115**, 216806 (2015).
9. Q. Ma *et al.*, Observation of the nonlinear Hall effect under time-reversal-symmetric conditions. *Nature* **565**, 337–342 (2019).
10. G. Kirchhoff, On a deduction of Ohm's laws, in connexion with the theory of electrostatics. *Philos. Mag.* **37**, 463–468 (1850).
11. A. Sommerfeld, E. G. Ramberg, *Electrodynamics (Lectures on Theoretical Physics,* Academic Press, New York, NY, 1952) vol. 3, pp. 125–133.
12. J. D. Jackson, Surface charges on circuit wires and resistors play three roles. *Am. J. Phys.* **64**, 855–870 (1996).
13. R. Müller, A semiquantitative treatment of surface charges in DC circuits. *Am. J. Phys.* **80**, 782–788 (2012).
14. M. J. Yoo *et al.*, Scanning single-electron transistor microscopy: Imaging individual charges. *Science* **276**, 579–582 (1997).
15. J. Martin *et al.*, Observation of electron–hole puddles in graphene using a scanning single-electron transistor. *Nat. Phys.* **4**, 144–148 (2008).
16. N. W. Ashcroft, N. D. Mermin, *Solid State Physics* (Holt, Rinehart and Winston, New York, NY, 1976), pp. 1–15.
17. K. S. Novoselov *et al.*, Electric field effect in atomically thin carbon films. *Science* **306**, 666–669 (2004).
18. K. S. Novoselov *et al.*, Two-dimensional gas of massless Dirac fermions in graphene. *Nature* **438**, 197–200 (2005).
19. Y. Zhang, Y.-W. Tan, H. L. Stormer, P. Kim, Experimental observation of the quantum Hall effect and Berry's phase in graphene. *Nature* **438**, 201–204 (2005).
20. Z. Tan *et al.*, Shubnikov-de Haas oscillations of a single layer graphene under dc current bias. *Phys. Rev. B* **84**, 115429 (2011).
21. L. Wang *et al.*, One-dimensional electrical contact to a two-dimensional material. *Science* **342**, 614–617 (2013).
22. J. Moser, A. Barreiro, A. Bachtold, Current-induced cleaning of graphene. *Appl. Phys. Lett.* **91**, 163513 (2007).
23. H. Wang, Y. Wu, C. Cong, J. Shang, T. Yu, Hysteresis of electronic transport in graphene transistors. *ACS Nano* **4**, 7221–7228 (2010).
24. E. J. H. Lee, K. Balasubramanian, R. T. Weitz, M. Burghard, K. Kern, Contact and edge effects in graphene devices. *Nat. Nanotechnol.* **3**, 486–490 (2008).
25. P. Blake *et al.*, Influence of metal contacts and charge inhomogeneity on transport properties of graphene near the neutrality point. *Solid State Commun.* **149**, 1068–1071 (2009).
26. Y. Zhang, V. W. Brar, C. Girit, A. Zettl, M. F. Crommie, Origin of spatial charge inhomogeneity in graphene. *Nat. Phys.* **5**, 722–726 (2009).
27. A. Allain, J. Kang, K. Banerjee, A. Kis, Electrical contacts to two-dimensional semiconductors. *Nat. Mater.* **14**, 1195–1205 (2015).
28. Q. G. Zhang, B. Y. Cao, X. Zhang, M. Fujii, K. Takahashi, Influence of grain boundary scattering on the electrical and thermal conductivities of polycrystalline gold nanofilms. *Phys. Rev. B* **74**, 134109 (2006).
29. S. Yoneoka *et al.*, Electrical and thermal conduction in atomic layer deposition nanobridges down to 7 nm thickness. *Nano Lett.* **12**, 683–686 (2012).
30. A. W. Tsen *et al.*, Tailoring electrical transport across grain boundaries in polycrystalline graphene. *Science* **336**, 1143–1146 (2012).
31. V. M. Pereira, A. H. Castro Neto, Strain engineering of graphene's electronic structure. *Phys. Rev. Lett.* **103**, 046801 (2009).
32. F. Guinea, M. I. Katsnelson, A. K. Geim, Energy gaps and a zero-field quantum Hall effect in graphene by strain engineering. *Nat. Phys.* **6**, 30–33 (2010).
33. F. J. Owens, Electronic and magnetic properties of armchair and zigzag graphene nanoribbons. *J. Chem. Phys.* **128**, 194701 (2008).
34. Y. M. Zuev, W. Chang, P. Kim, Thermoelectric and magnetothermoelectric transport measurements of graphene. *Phys. Rev. Lett.* **102**, 096807 (2009).
35. D. Xiao, M.-C. Chang, Q. Niu, Berry phase effects on electronic properties. *Rev. Mod. Phys.* **82**, 1959–2007 (2010).